

Supplementary material to *Determining the optimal structural resolution of proteins through an information-theoretic analysis of their conformational ensemble*

Margherita Mele,^{1,2} Raffaele Fiorentini,^{1,2} Thomas Tarenzi,³ Giovanni Mattiotti,^{1,2,4} and Raffaello Potestio^{1,2}

¹*Physics Department, University of Trento, via Sommarive, 14 I-38123 Trento, Italy*

²*INFN-TIFPA, Trento Institute for Fundamental Physics and Applications, I-38123 Trento, Italy*

³*School of Chemistry, University of Birmingham, B15 2TT Birmingham, UK*

⁴*Unité de Biologie Fonctionnelle et Adaptative, CNRS UMR 8251, Inserm ERL U1133, Université Paris Cité, 35 rue Hélène Brion, Paris, France*

(Dated: October 16, 2025)

This file contains complementary material to the main manuscript. It includes methodological details on the computation of the reported quantities, the full list of parameters used, and supplementary analyses. Figures and tables are provided to document additional results that are omitted from the main text for conciseness.

- Section I: Description of the numerical procedure used to identify the optimal number of retained atoms from the relevance–resolution curve.
- Section II: Complete PROPRES outputs, input parameters, and simulation settings for both adenylylate kinase and the 11-protein dataset.
- Section III: Linear scaling of optimal resolution with protein size and comparison with MARTINI and SIRAH coarse-grained models.
- Section IV: Protein-specific analysis of the covariance matrix and identification of the elbow point associated with structural fluctuations.
- Section V: Protein-specific analysis of mapping entropy and variance profiles, relating information loss to coarse-graining resolution.

I. IDENTIFICATION OF THE OPTIMAL NUMBER OF RETAINED SITES

Once the relevance-resolution plot is constructed, the next step consists of identifying the point where the curve has slope $\mu = -1$, that is the point of optimal trade-off between detail parsimony and information gain. This is a tricky step, in that we do not have a smooth, differentiable curve, but rather a scatter plot of points distributed on a range in both resolution and relevance. For simplicity, we describe the procedure with reference to the target slope -1 , but both the method and the implementation are general and can be applied to identify points corresponding to any desired slope, for instance, a slope of 0 corresponding to the maximum of relevance.

In order to identify this soft spot and find the number of retained atoms that best corresponds to it, one can proceed in at least two particularly intuitive ways: the *uniform density* and the *uniform spacing* averaging protocols. Each of the two consists in a rule to group the points that fall into the same, predefined resolution interval, and associate a single value of the relevance to each bin.

In the *uniform density* protocol, points are grouped so that every resolution interval contains the same number D of $(H_{\text{res}}, H_{\text{rel}})$ points: in this way, a uniform distribution of points is promoted by construction, and the value of the relevance, obtained averaging over the points in the bin, has a statistical weight comparable to that of the others. The default value of D is set to 100 , but can be changed by the user. In Fig. 1 we illustrate the outcome of this procedure applied to a dataset of 30 points that we built *ad hoc* for a pictorial representation; here, we chose to set the number of points per bin $D = 5$ in order to have a sufficient number of both points and bins.

In contrast, in the *uniform spacing* protocol the x axis is subdivided in W intervals of width $1/W$, in order to promote a uniformly-distributed coverage of the resolution range. The default value of W is 100 . Its application is illustrated in Fig. 2, where the number of windows has been set so as to have the same number of bins as in the previous case.

The choice of the method might depend on the specific necessity; in the applications explored in this work, the uniform density protocol is preferable as it returns a finer distribution of points in the region of interest to the PROPRES protocol, *i.e.* on the right of the maximum of H_{rel} . The outcome of this smoothing procedure is a sequence of representative points, whose resolution value is given by the midpoint of the bins, and the relevance is given by the average of the points in the bin. Such representative points are indicated with red circles in Figs. 1 and 2.

Then, the program computes the numerical derivative of the curve of representative points. The method employed is the simple Newton’s difference quotient. Once the derivative is known, the algorithm highlights the points that correspond to a slope in the interval $[-1.1, -0.9]$ (as pictorially represented in Fig. 3), a reasonable compromise between being accurately close to -1 and accounting for a function defined by a small and finite number of points. For all points in this slope range, the associated numbers of retained heavy atoms are collected, and a histogram is built to count their occurrences. The mean and standard deviation of this distribution are used to define the optimal number of retained atoms, N_{OPT} , and its uncertainty (see Fig. 3c,d). For each value of N_{CG} , resolution and relevance are computed over 50 randomly generated mappings. Although this represents a negligible fraction of all possible N_{CG} -atom selections from the n_{ha} available atoms, this sample size was found to be sufficient in practice to obtain stable average values.

As noted above, the slope-identification procedure is

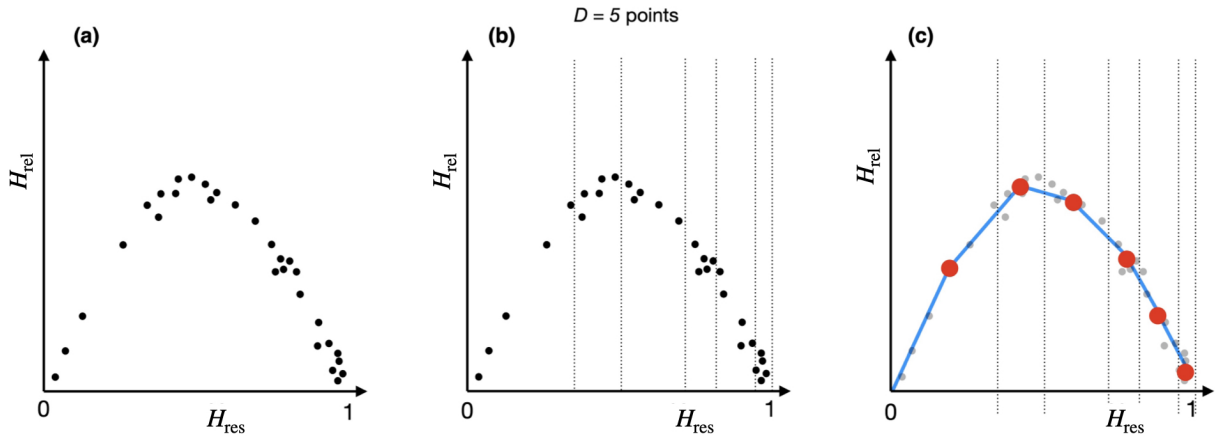


Figure 1. Uniform density approach to binning resolution-relevance curves. (a) pictorial representation of 30 relevance and resolution points that we built *ad hoc* for a pictorial representation; (b) subdivision of the x axis into intervals of variable width, each one containing 5 points ($D = 5$); (c) average curve of relevance and resolution (red circles and blue lines).

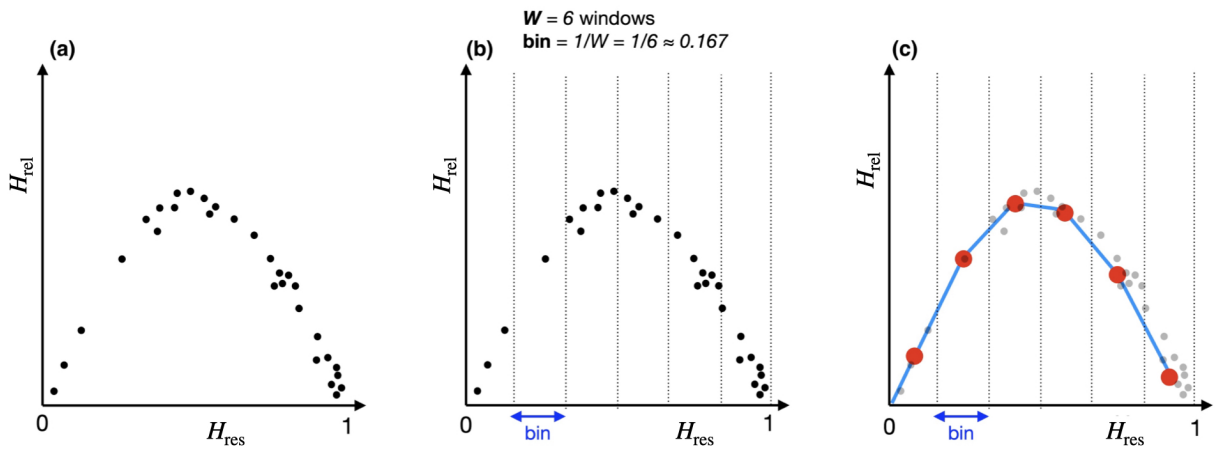


Figure 2. Uniform spacing approach to binning resolution-relevance curves. (a) pictorial representation of 30 relevance and resolution points that we built *ad hoc* for a pictorial representation; (b) subdivision of the x axis into 6 intervals of same length ($W = 6$, bin width $1/W$), each one containing a variable number of points; (c) average curve of relevance and resolution (red circles and blue lines).

general; in this work we employ two operational definitions. First, the point at slope $\mu = -1$, which marks the information–theoretic balance between resolution and relevance (i.e., where the marginal gain in relevance equals the marginal cost in resolution); the associated number of retained atoms is denoted $N_{\text{OPT}}^{\text{IT}}$. Second, the point at slope $\mu = 0$, corresponding to the maximum of relevance; the associated number is denoted $N_{\text{OPT}}^{\text{MR}}$. Both $N_{\text{OPT}}^{\text{IT}}$ and $N_{\text{OPT}}^{\text{MR}}$ provide complementary reference scales for characterising the information content of coarse-grained representations.

II. PROPRE OUTPUTS AND PARAMETERS

In this section, we report the complete outputs of the PROPRE workflow together with the simulation parameters used. The analysis was performed both on the adenylate kinase (ake) trajectories and on a dataset of eleven additional proteins. The simulation parameters for ake are summarized in Table I, while those for the dataset are given in Table II. For each trajectory, 1000 frames were analyzed. In the case of ake, these frames were equally spaced along the trajectory. For the dataset proteins, we considered two complementary sampling schemes: a strided trajectory composed of 1000 equally spaced frames and a clustered trajectory composed of 1000 frames corresponding to the centroids of a UPGMA clusterization. As per the default software settings, 50 random mappings were generated for each fixed number of coarse-grained (CG) sites, and the number of retained atoms was progressively reduced in increments of 0.5% of the total protein heavy atoms; the corresponding numbers of CG sites are reported in the tables. The resulting relevance–resolution curves were smoothed using the uniform density protocol, which employs d points per resolution bin. Optimal bins were identified when their slopes fell within the confidence intervals around the target slopes: s_{-1} denotes the confidence interval for $\tilde{\mu} = -1$, while s_0 corresponds to that for $\tilde{\mu} = 0$. The full results of the PROPRE workflow are displayed in Figure 4-6 for AKE and in Figure 7-17 for the dataset proteins. All figures share the same organization: panels (a,e) display resolution–relevance scatter plots, with density-averaged curves shown in black and pink rectangles marking the regions near the target slopes; panels (b,f) provide close-up views of the highlighted regions; panels (c,g) report the numerical slope $\tilde{\mu}$ as a function of the point index, with the slope-selection interval shaded in pink; and panels (d,h) show histograms of the number of retained sites $N_{\text{CG}}^{(i)}$, where vertical red lines indicate the mean values N_{opt} and the shaded pink areas correspond to \pm one standard deviation.

Protein	N_{at}	N_{sites}	d	s_{-1}	s_0
ake-full	1656	207	170	10%	10%
ake-closed	1656	207	170	10%	10%
ake-open	1656	207	170	10%	10%

Table I. PROPRE Parameters. This table lists the parameters used in the analysis: the protein identifier, the number of protein heavy atoms (N_{at}), the number of coarse-grained sites (N_{sites}), the number of points per resolution bin (d), and the confidence interval bounds for optimal bin selection, with s_{-1} corresponding to a target slope of -1 and s_0 corresponding to a target slope of 0 .

Protein	N_{at}	N_{sites}	d	s_{-1}	s_0
STRIDING					
ligd	434	216	100	10%	10%
1knt	440	219	110	10%	10%
1qke	473	235	100	10%	20%
1hyp	539	268	100	10%	10%
1dsl	706	235	100	10%	20%
1noa	761	253	100	15%	10%
1une	957	239	100	10%	10%
1sno	1090	218	100	10%	10%
1koe	1310	218	100	10%	10%
2exo	2400	200	100	10%	10%
1xwl	4654	203	150	10%	10%
CLUSTERING					
ligd	434	216	110	10%	10%
1knt	440	219	110	15%	10%
1qke	473	235	100	10%	20%
1hyp	539	268	120	10%	10%
1dsl	706	235	140	10%	20%
1noa	761	253	130	15%	10%
1une	957	239	100	10%	10%
1sno	1090	218	110	10%	10%
1koe	1310	218	110	10%	15%
2exo	2400	200	100	10%	10%
1xwl	4654	203	100	10%	10%

Table II. PROPRE Parameters. This table lists the parameters used in the analysis: the protein identifier, the number of protein heavy atoms (N_{at}), the number of coarse-grained sites (N_{sites}), the number of points per resolution bin (d), and the confidence interval bounds for optimal bin selection, with s_{-1} corresponding to a target slope of -1 and s_0 corresponding to a target slope of 0 .

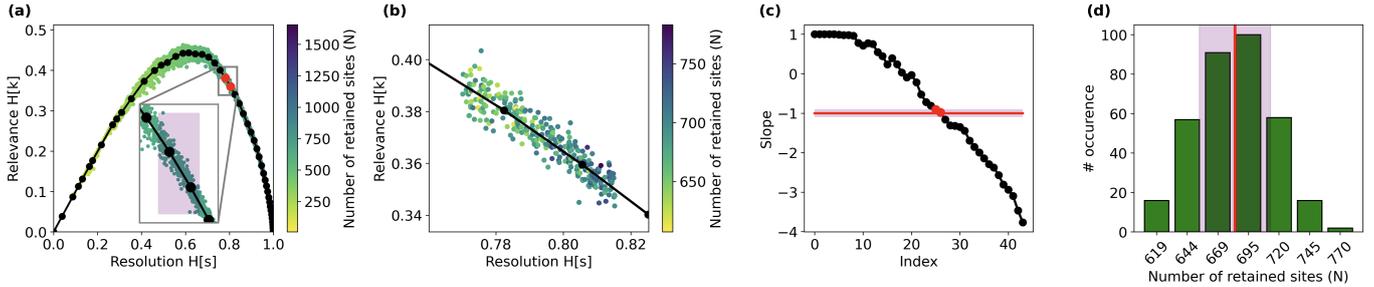


Figure 3. Summary of the PROPRES workflow applied to a 500 ns simulation of adenylate kinase (details in the Results section). **(a)** Resolution–relevance scatter plot. The black curve is the average obtained using a density-based protocol ($d = 170$). The pink rectangle highlights the region where the slope $\tilde{\mu}$ falls within $[-1.1, -0.9]$. **(b)** Numerical slope $\tilde{\mu}$ versus point index, with the interval $[-1.1, -0.9]$ shown in pink. Although only two points meet this slope criterion, they correspond to multiple possible numbers of retained atoms. **(c)** Close-up of the points in the pink rectangle from panel (a). **(d)** Histogram of the various numbers of retained sites $N_{CG}^{(i)}$. The vertical red line marks the mean value, N_{OPT} , and the shaded pink region indicates \pm one standard deviation around it.

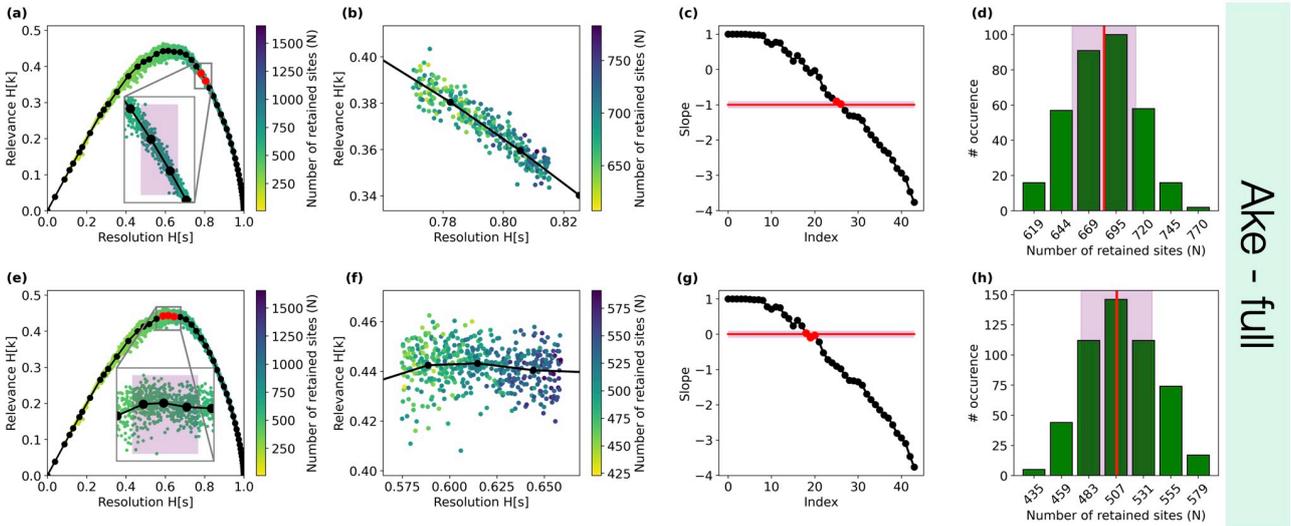


Figure 4. Summary of the PROPRES workflow applied to ake full trajectory for two target slopes, $\tilde{\mu} = -1$ (top row) and $\tilde{\mu} = 0$ (bottom row).

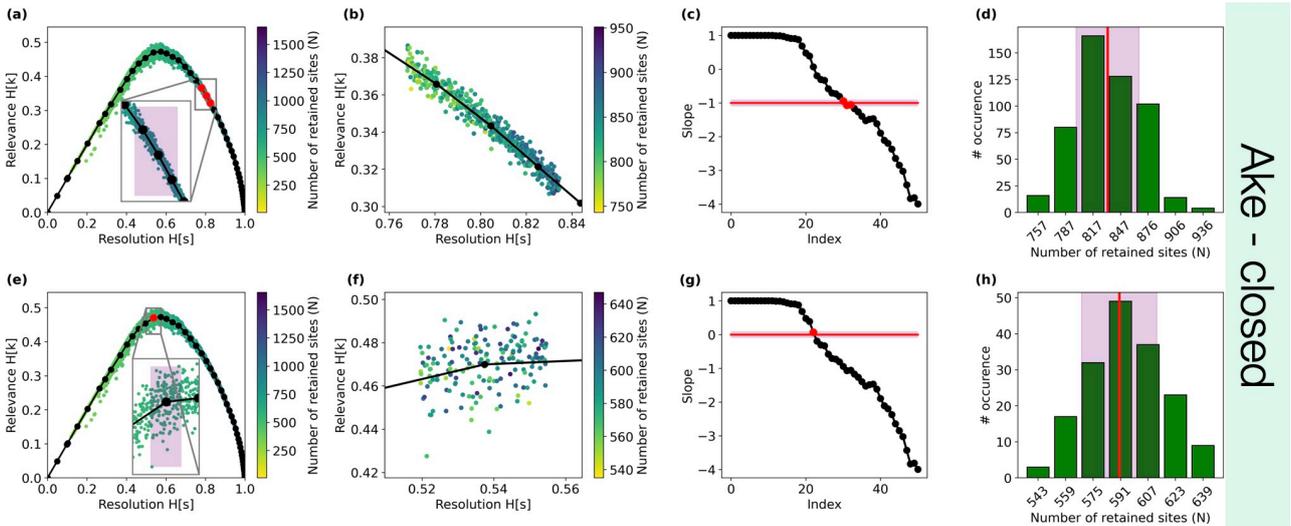


Figure 5. Summary of the PROPRES workflow applied to ake closed cluster for two target slopes, $\tilde{\mu} = -1$ (top row) and $\tilde{\mu} = 0$ (bottom row).

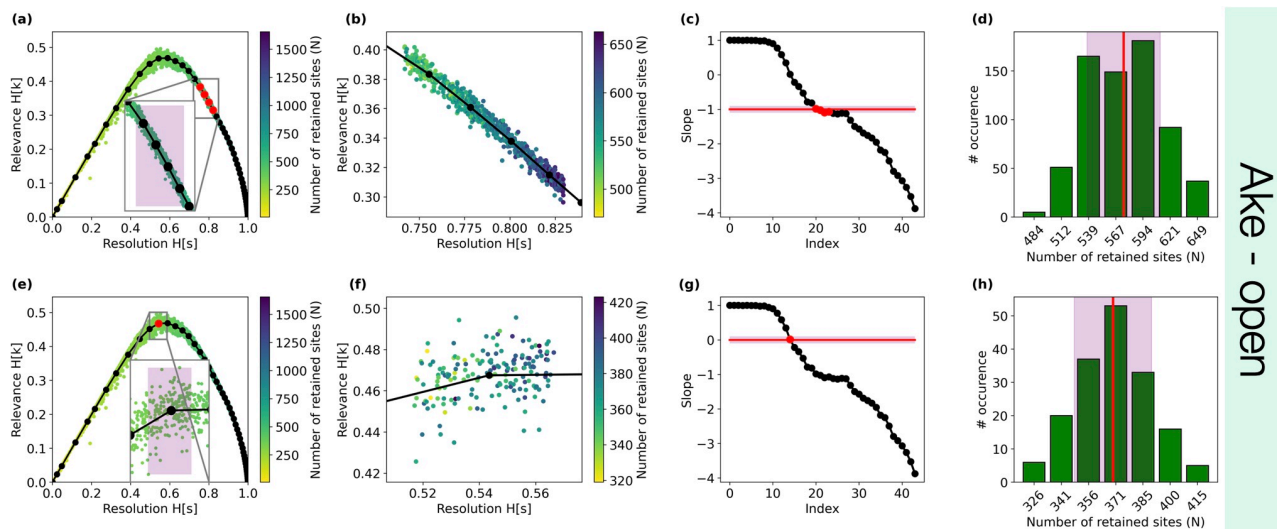


Figure 6. Summary of the PROPRES workflow applied to ake open cluster for two target slopes, $\tilde{\mu} = -1$ (top row) and $\tilde{\mu} = 0$ (bottom row).

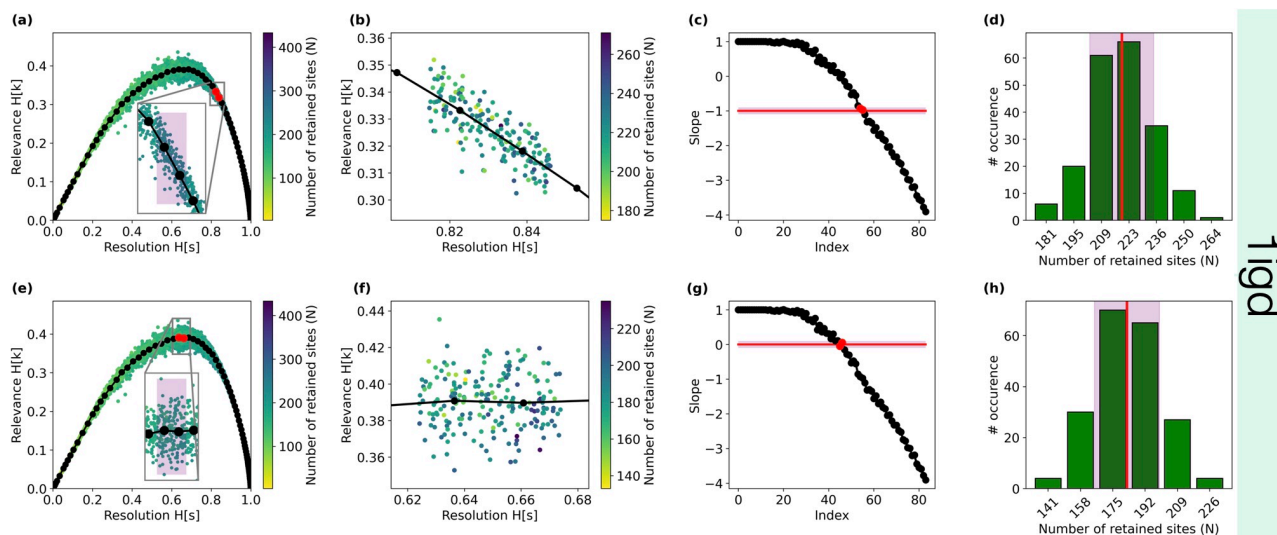


Figure 7. Summary of the PROPRES workflow applied to 1igd trajectory for two target slopes, $\tilde{\mu} = -1$ (top row) and $\tilde{\mu} = 0$ (bottom row).

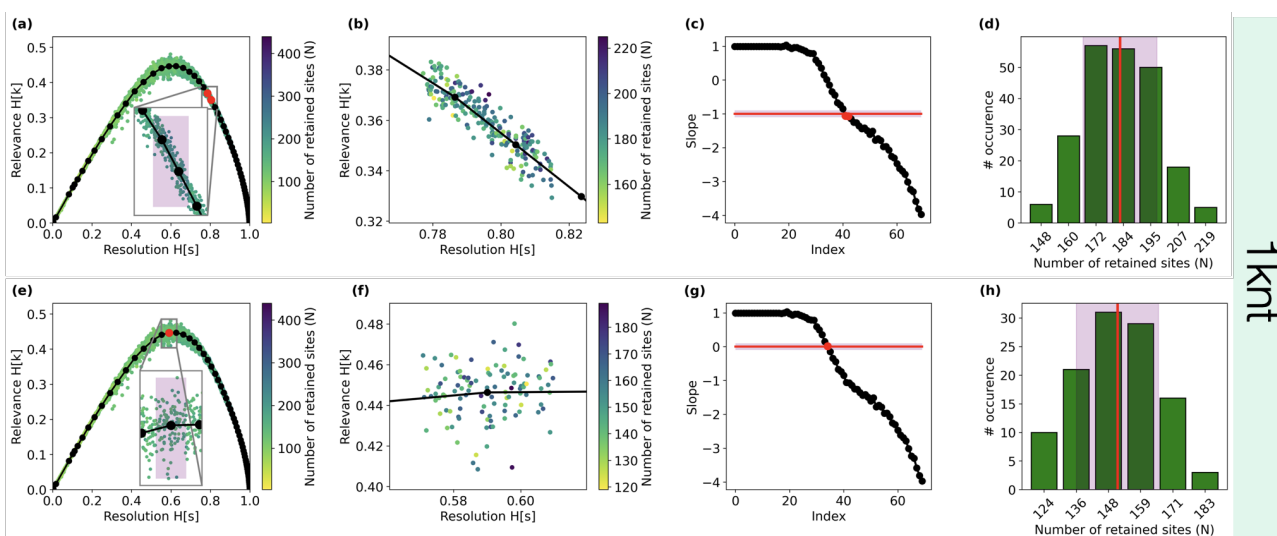


Figure 8. Summary of the PROPRES workflow applied to 1knt trajectory for two target slopes, $\tilde{\mu} = -1$ (top row) and $\tilde{\mu} = 0$ (bottom row).

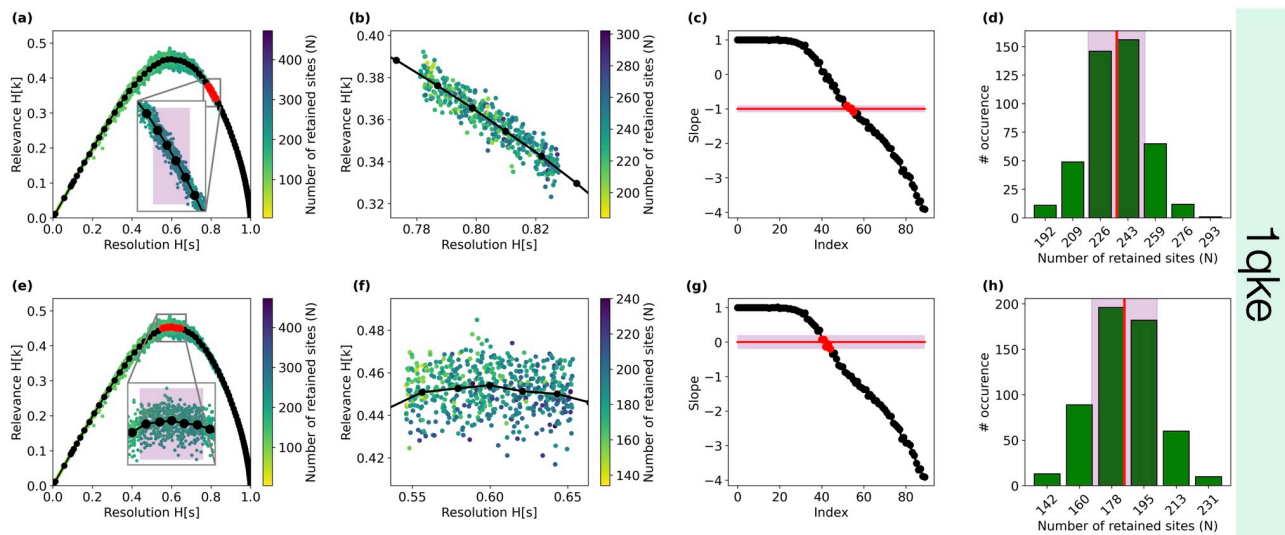


Figure 9. Summary of the PROPRES workflow applied to 1qke trajectory for two target slopes, $\tilde{\mu} = -1$ (top row) and $\tilde{\mu} = 0$ (bottom row).

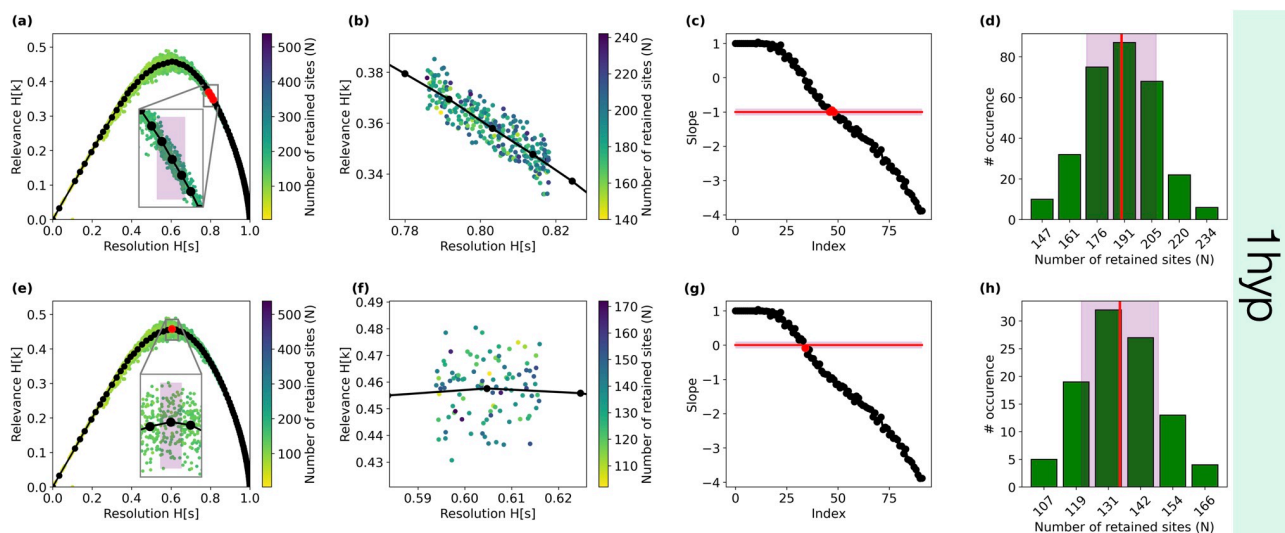


Figure 10. Summary of the PROPRES workflow applied to 1hyp trajectory for two target slopes, $\tilde{\mu} = -1$ (top row) and $\tilde{\mu} = 0$ (bottom row).

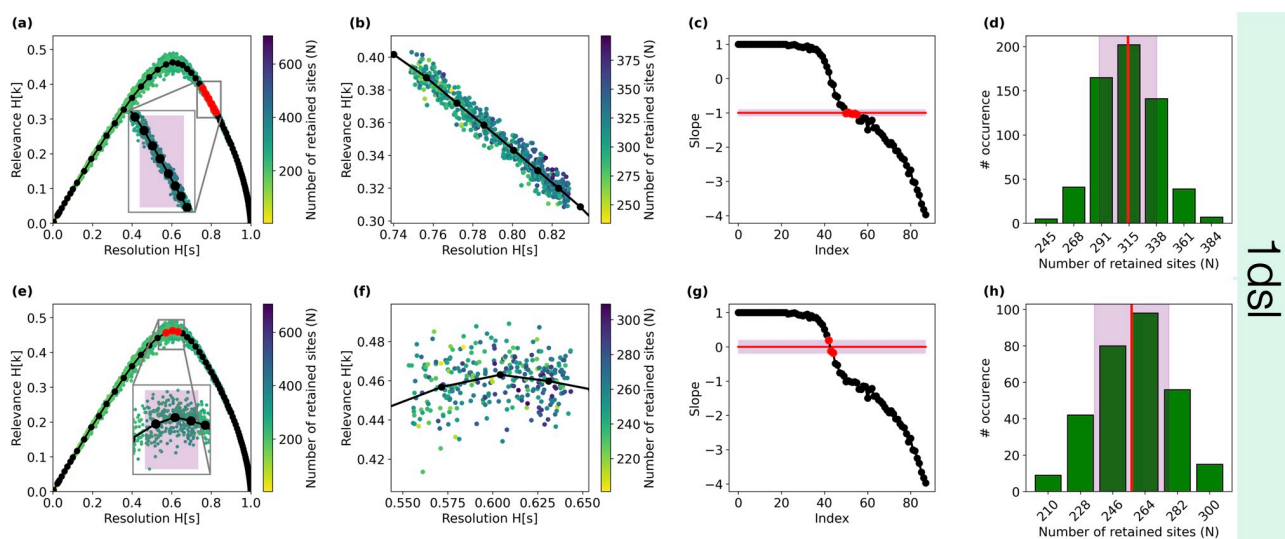


Figure 11. Summary of the PROPRES workflow applied to 1dsl trajectory for two target slopes, $\tilde{\mu} = -1$ (top row) and $\tilde{\mu} = 0$ (bottom row).

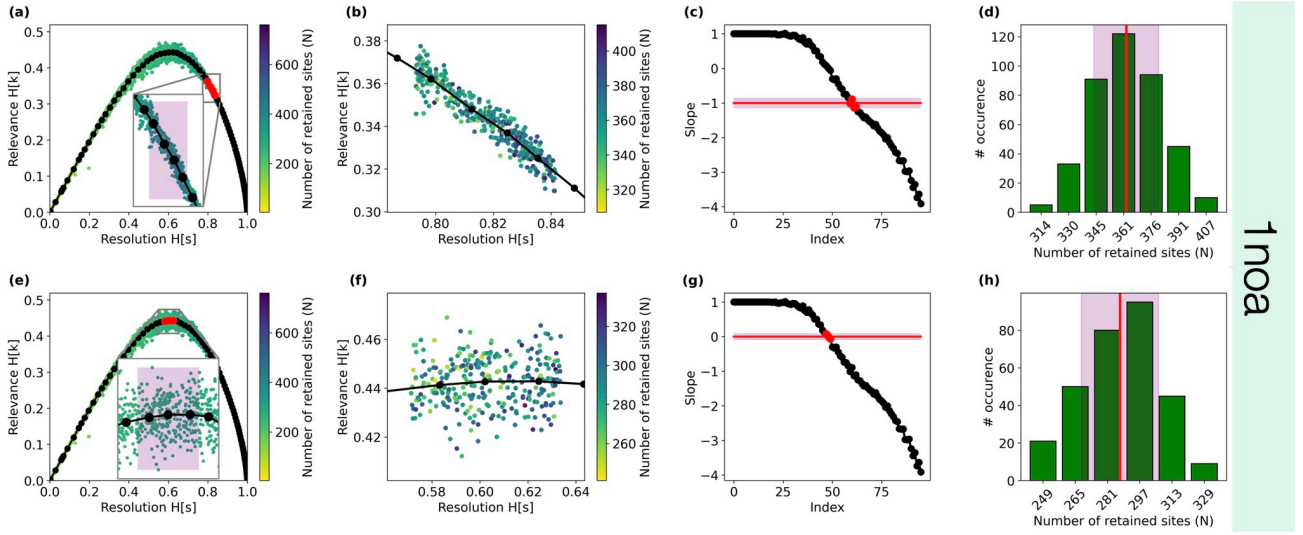


Figure 12. Summary of the PROPRES workflow applied to 1noa for two target slopes, $\tilde{\mu} = -1$ (top row) and $\tilde{\mu} = 0$ (bottom row).

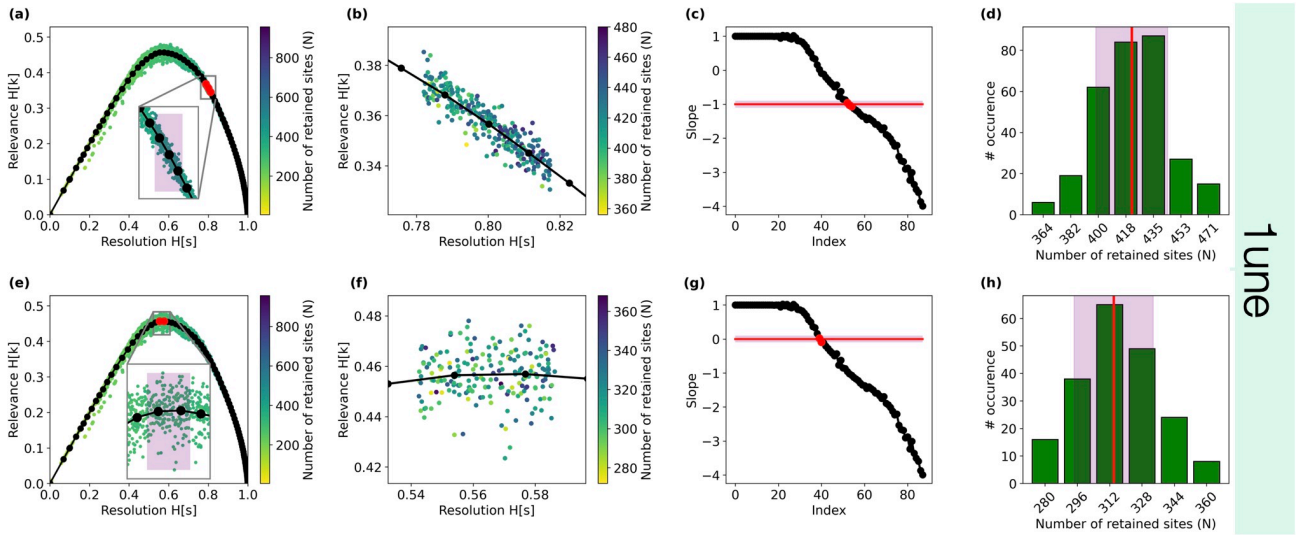


Figure 13. Summary of the PROPRES workflow applied to 1une trajectory for two target slopes, $\tilde{\mu} = -1$ (top row) and $\tilde{\mu} = 0$ (bottom row).

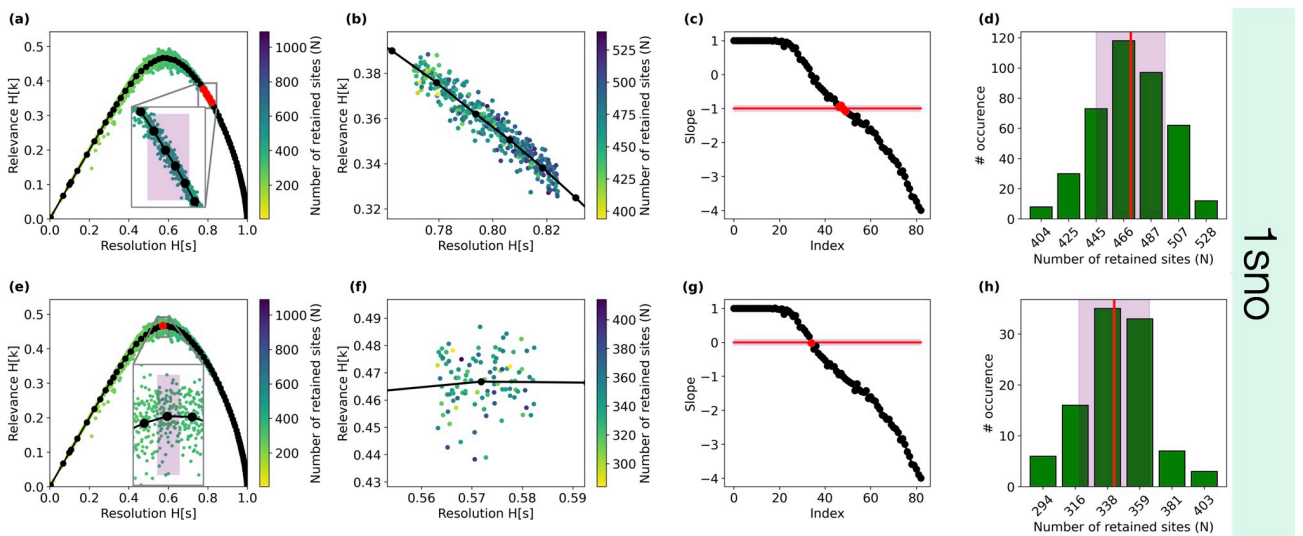


Figure 14. Summary of the PROPRES workflow applied to 1sno trajectory for two target slopes, $\tilde{\mu} = -1$ (top row) and $\tilde{\mu} = 0$ (bottom row).

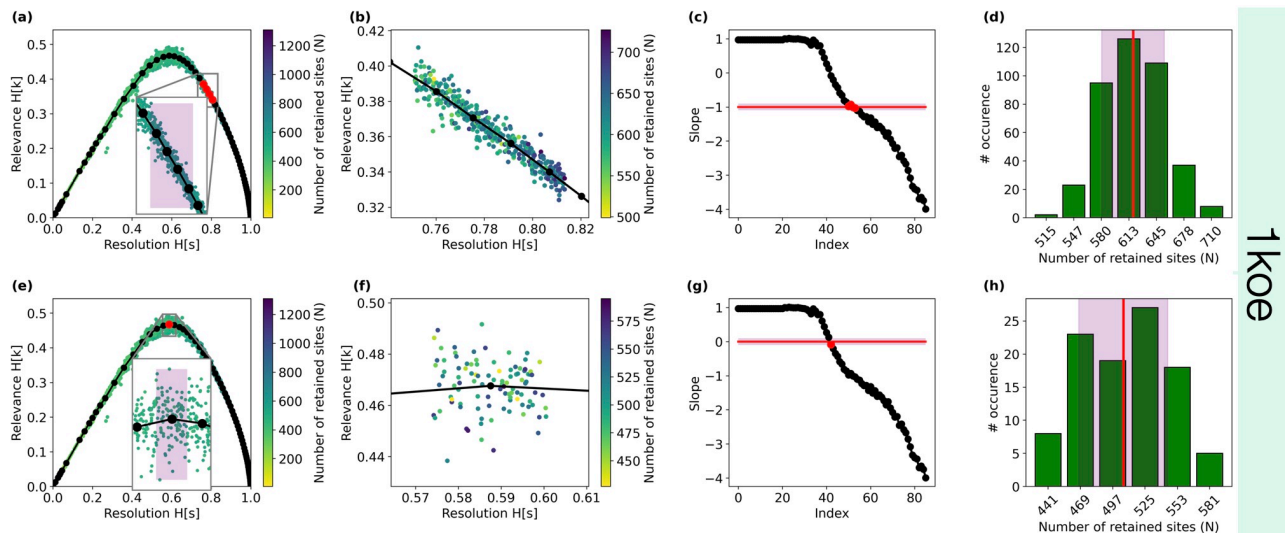


Figure 15. Summary of the PROPRES workflow applied to 1koe trajectory for two target slopes, $\tilde{\mu} = -1$ (top row) and $\tilde{\mu} = 0$ (bottom row).

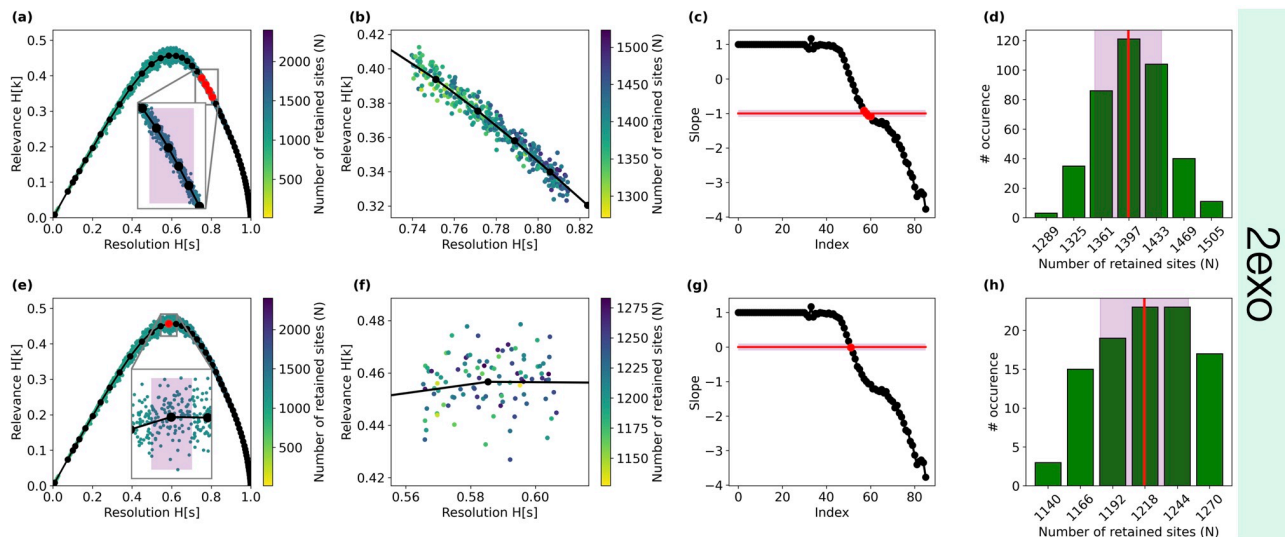


Figure 16. Summary of the PROPRES workflow applied to 2exo trajectory for two target slopes, $\tilde{\mu} = -1$ (top row) and $\tilde{\mu} = 0$ (bottom row).

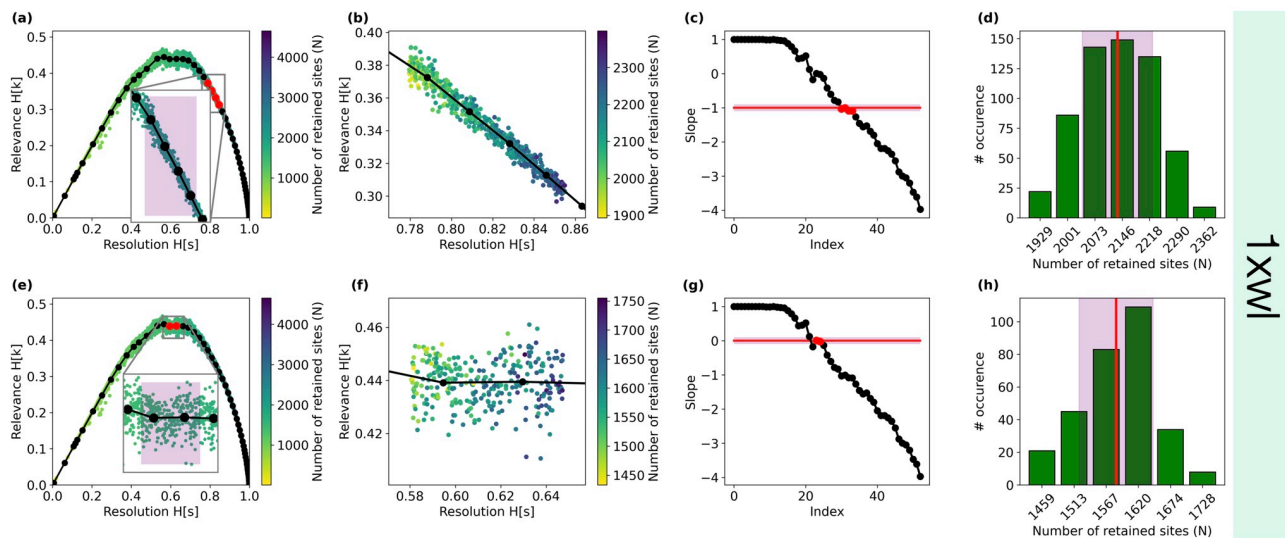


Figure 17. Summary of the PROPRES workflow applied to 1xwl trajectory for two target slopes, $\tilde{\mu} = -1$ (top row) and $\tilde{\mu} = 0$ (bottom row).

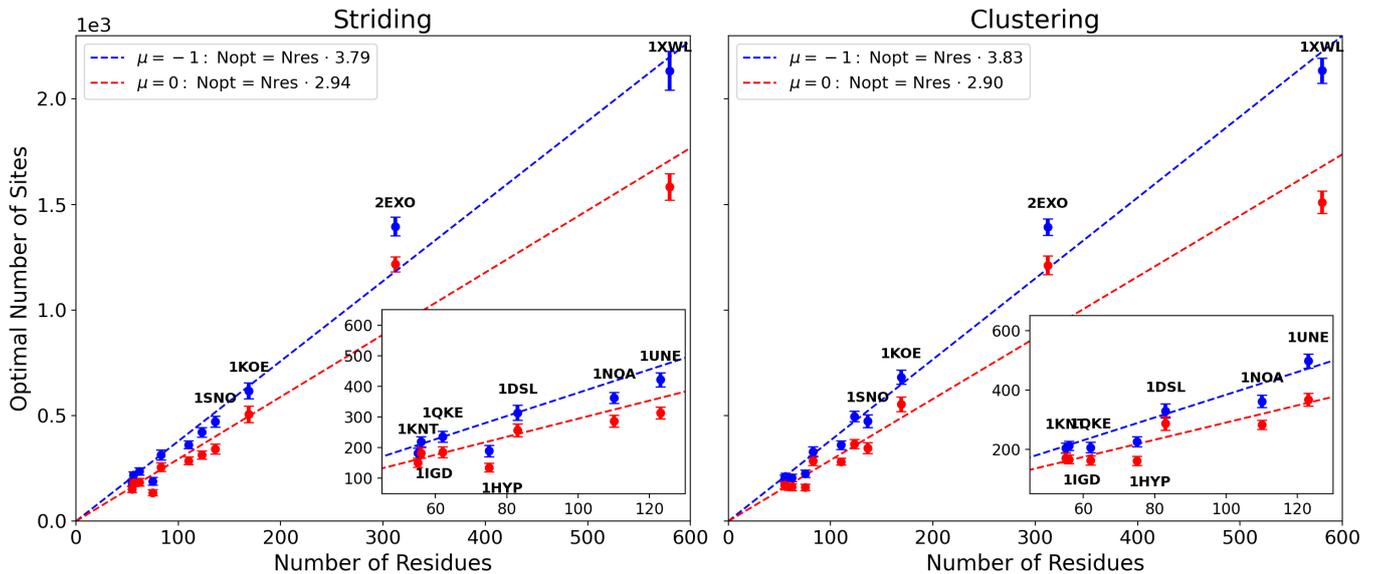


Figure 18. Scatter plots showing the optimal number of sites identified by PROPRES as a function of the number of residues for various proteins. The left panel (*Striding*) uses 1000 equidistant frames from the trajectory, while the right panel (*Clustering*) uses the centroids of 1000 clusters obtained from a clustering procedure. Blue markers represent the number of sites corresponding to a slope of -1 in the relevance resolution curve ($\mu = -1$), whereas red markers indicate the number of sites where relevance is maximized ($\mu = 0$). Error bars denote standard deviations. Dashed lines show linear fits, with the indicated proportionality constants between the optimal number of sites (N_{opt}) and the number of residues (N_{res})

III. 11-PROTEINS FIT

In the main text, we discuss how the PROPRES algorithm identifies the optimal resolution for each protein—defined as the heavy atom fraction minimising the information loss upon coarse-graining—and reported a clear linear relationship between the optimal number of sites (N_{OPT}) and the total number of residues (n_{AA}) when evaluated at $\mu = -1$. The analysis can be also extended to the point $\mu = 0$, i.e., the point where the relevance is maximised. This point corresponds to a further reduction in the resolution, which in turn yields a gain in relevance content. As shown in Fig.18, the linear scaling between N_{OPT} and n_{AA} is also preserved in this case, with comparable correlation coefficients ($R \approx 0.99$ for both striding and clustering).

The slope of the linear fit decreases from about 3.8 at $\mu = -1$ to about 2.9 at $\mu = 0$, meaning that the number of retained atoms per residue is lower. Taken together, these two values define a range of meaningful resolutions for globular proteins, spanning from detailed representations that better preserve structural information ($\mu = -1$) to coarser yet still representative descriptions at maximum relevance ($\mu = 0$).

To quantitatively compare the optimal resolutions identified by PROPRES with those adopted in widely used coarse-grained (CG) force fields, we computed for each protein in the dataset the ratio between the number of beads employed by the MARTINI and SIRAH models and the optimal number of retained sites predicted by PROPRES. Both definitions of optimal resolution are considered: the information-theoretic estimate ($N_{\text{OPT}}^{\text{IT}}$, slope $\mu = -1$) and the relevance-maximum estimate ($N_{\text{OPT}}^{\text{RM}}$, slope $\mu = 0$). Results are reported in Fig. 19 for both trajectory sampling strategies (striding and clustering). In all cases, the MARTINI mapping (blue) corresponds on average to about 0.6–0.8, N_{OPT} , whereas SIRAH (orange) employs a finer resolution, with ratios in the range 1.3–1.7, N_{OPT} depending on the sampling method and the definition of optimal resolution. The consistency of these ratios across proteins and sampling strategies confirms that the effective resolutions of MARTINI and SIRAH fall within the range identified by PROPRES as meaningful for globular proteins.

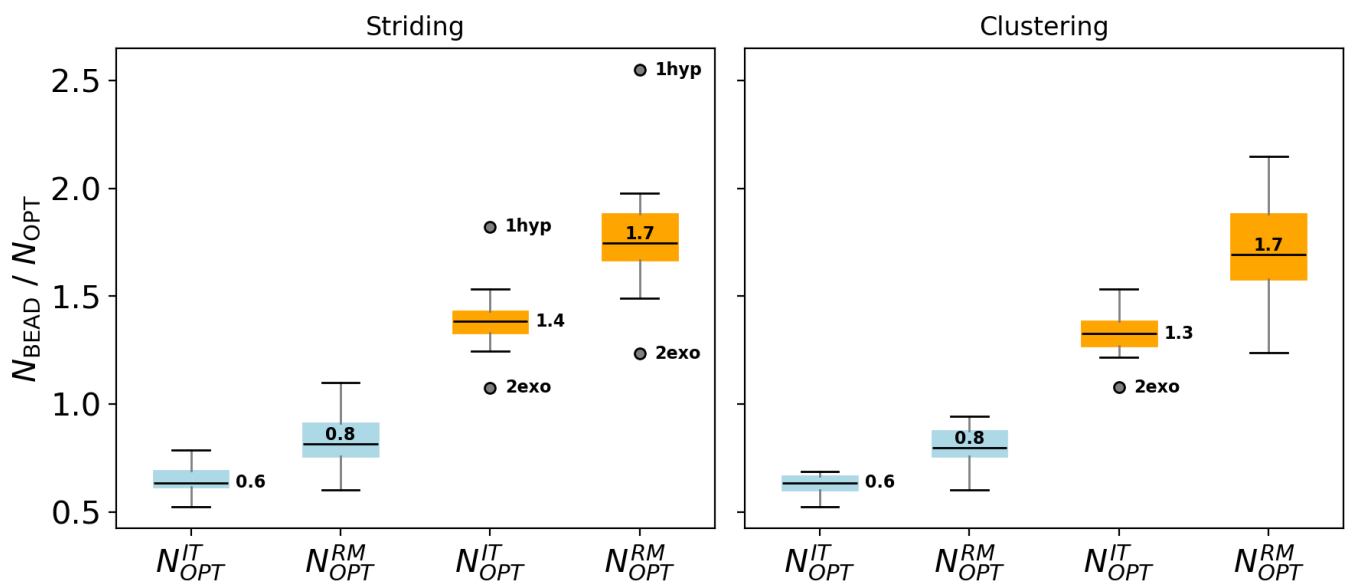


Figure 19. Ratio between the number of coarse-grained beads used by the MARTINI (blue) and SIRAH (orange) models and the optimal number of retained sites N_{OPT} identified by PROPRE, for the 11 proteins in the dataset. Left and right panels correspond to the striding and clustering sampling strategies, respectively. For each model, two boxplots are shown: the first refers to the information-theoretic estimate ($N_{\text{OPT}}^{\text{IT}}$, slope $\mu = -1$) and the second to the relevance-maximum estimate ($N_{\text{OPT}}^{\text{RM}}$, slope $\mu = 0$). Boxes indicate the interquartile range and median (bold line), with individual protein outliers labeled. Numerical values above each box denote the median ratio.

IV. COVARIANCE MATRIX

For each of the 11 proteins in the dataset, we report the detailed analysis of the relationship between the normalized covariance (cov) and the number of retained atoms (N_{CG}), together with the corresponding variance curves $\sigma_{cov}^2(N_{CG})$ (Fig. 20). In each case, the elbow position (N_{CG}^E) is identified from the fitted decay of the variance, while the optimal resolutions determined by PROPRES (N_{OPT}^{IT} and N_{OPT}^{MR}) are indicated for comparison.

The results consistently show that the variance of cov decreases with increasing N_{CG} , displaying an elbow-shaped trend whose position strongly correlates with the optimal resolutions identified by PROPRES. For all proteins, the optimal range lies just beyond the elbow point, indicating that PROPRES systematically selects resolutions sufficient to capture the dominant structural fluctuations while minimizing information loss.

V. MAPPING ENTROPY

For each of the 11 proteins in the dataset, we report the complete analysis of the mapping entropy (S_{map}) and its variance ($\sigma_{S_{map}}^2$) as a function of the number of retained atoms (N_{CG}) (Fig. 21). In each case, S_{map} was evaluated over 50 random selections of heavy atoms for each coarse-graining level, while the smoothed variance profile ($S_{S_{map}}^2$) was obtained by applying a Gaussian filter with a standard deviation of 5. The position of the variance peak (N_{CG}^P) is reported together with the optimal resolutions determined by PROPRES, N_{OPT}^{IT} and N_{OPT}^{MR} .

The results confirm for all proteins that S_{map} decreases smoothly with increasing N_{CG} , while its variance exhibits a pronounced maximum at intermediate resolutions. The peak of $S_{S_{map}}^2$ consistently falls close to the resolution range identified by PROPRES, indicating that the most informative coarse-grained representations correspond to the regime where the sensitivity of information retention to atom selection is maximal.

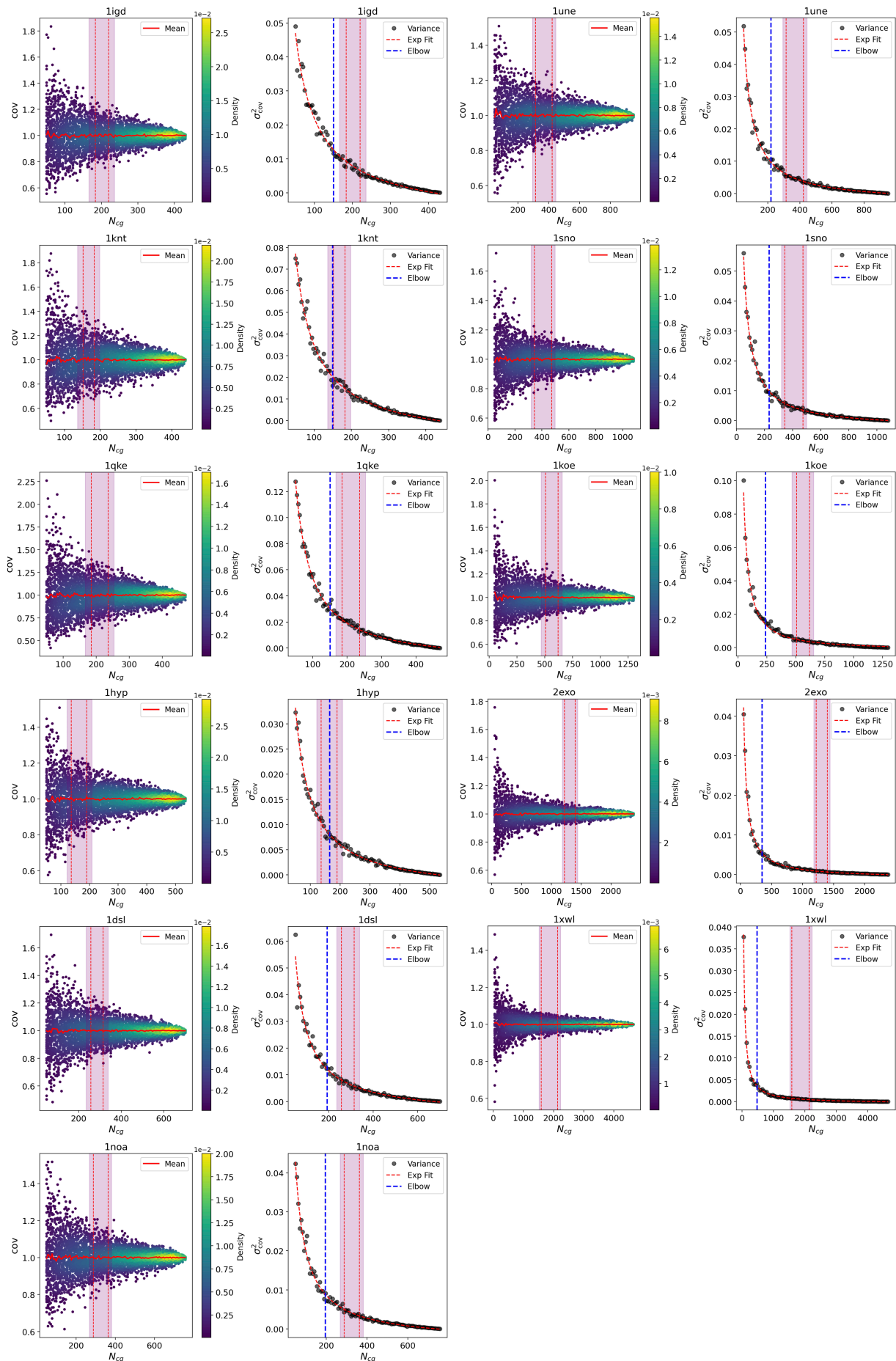


Figure 20. Detailed analysis of the normalized covariance (cov) and its variance $\sigma_{\text{cov}}^2(N_{\text{CG}})$ for all 11 proteins in the dataset. For each protein, the left panel shows the distribution of cov as a function of the number of retained atoms N_{CG} , with the red line representing the running average. The right panel displays the corresponding variance $\sigma_{\text{cov}}^2(N_{\text{CG}})$ (gray points) and its fitted decay (red line). Vertical blue dashed lines mark the elbow position (N_{CG}^E), while vertical red dashed lines and shaded regions indicate the optimal resolution range identified by PROPRES ($N_{\text{OPT}}^{\text{IT}}$ and $N_{\text{OPT}}^{\text{MR}}$).

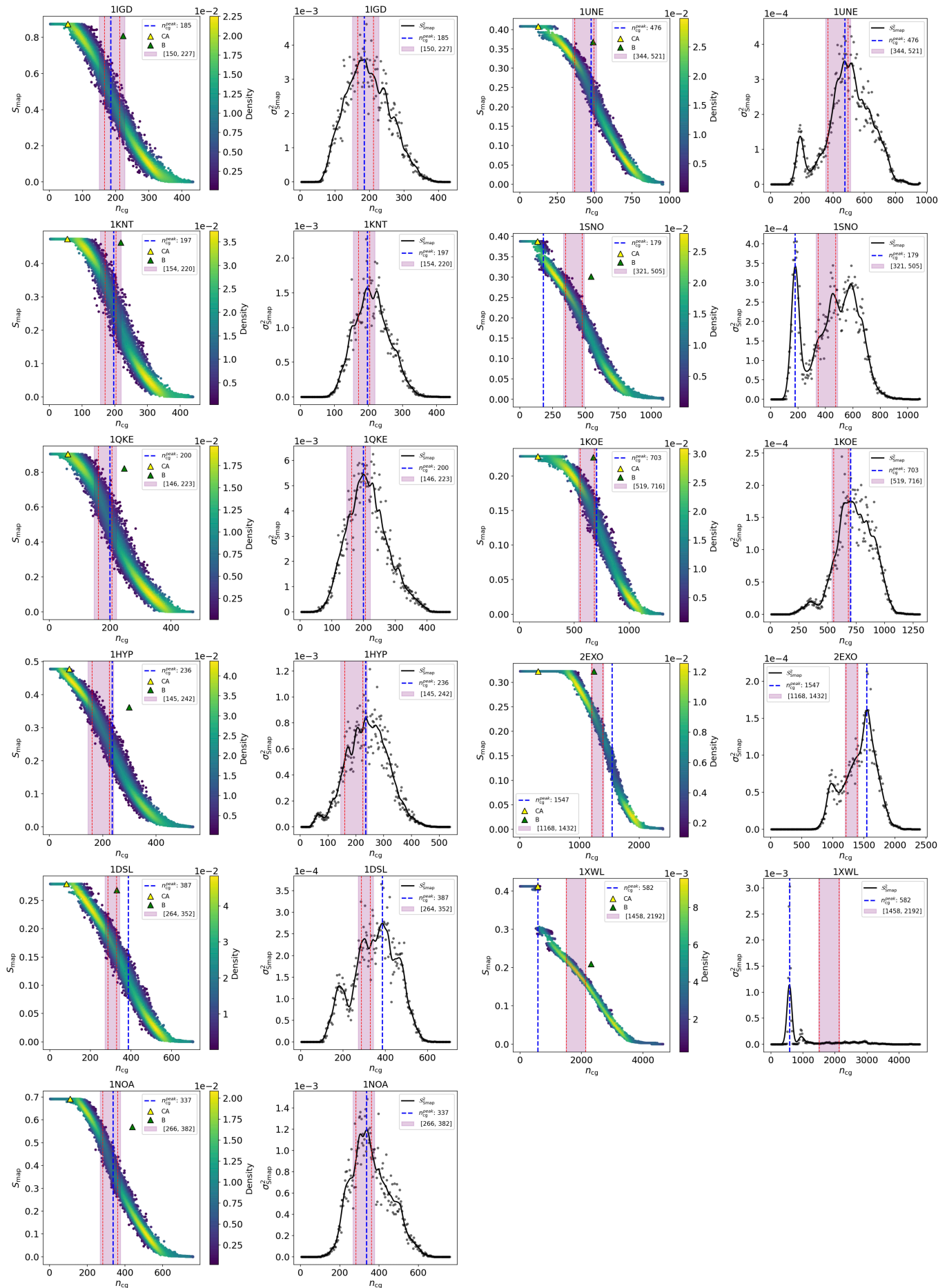


Figure 21. Detailed analysis of the mapping entropy (S_{map}) and its variance $\sigma_{S_{\text{map}}}^2(N_{\text{CG}})$ for all 11 proteins in the dataset. For each protein, the left panel shows the distribution of S_{map} as a function of the number of retained atoms N_{CG} , computed over 50 random subsets of heavy atoms; color encodes the pointwise density. The right panel reports the corresponding variance $\sigma_{S_{\text{map}}}^2(N_{\text{CG}})$ (gray points) and its Gaussian-smoothed profile $S_{S_{\text{map}}}^2$ (black line). Vertical blue dashed lines indicate the position of the variance peak (N_{CG}^P), while vertical red dashed lines and shaded regions mark the optimal resolution range identified by PROPRE ($N_{\text{OPT}}^{\text{IT}}$ and $N_{\text{OPT}}^{\text{MR}}$).